Ramírez-Uribe, I., Siebe, C., Chevrel, M.O., Ferres, D., and Salinas, S., 2021, The late Holocene Nealtican lava-flow field, Popocatépetl volcano, central Mexico: Emplacement dynamics and future hazards: GSA Bulletin, https://doi.org/10.1130/B36173.1.

Supplemental Material

Supplemental Material 1.

Table S1. Whole rock major (wt%) and trace element (ppm) analyses of Nealtican lava and Lorenzo pumice rock samples from Popocatépetl volcano.

Supplemental Material 2.

Table S2. Average compositions of glass and minerals in rocks from Popocatépetl volcano (Nealtican lava flows).

Supplemental Material 3. Methods for geothermobarometric and hygrometric calculations.

Table S3. Thermo-barometry and hygrometry calculation results for Popocatépetl volcano (Nealtican lava flows).

Supplemental Material 4. Methods for estimating rheological properties of lava flows and their emplacement times.

Table S4. Recalculated chemical composition of the residual liquid after crystallization of phenocrysts.

Table S5. Magma and lava viscosities of Nealtican lava flows for pre- and *syn*-eruption conditions, calculated following the petrological approach that accounts for the chemical composition of the bulk rock and the residual liquid, thermo-barometry, hygrometry, and crystal volume.

Supplemental Material 3.

METHODS FOR GEOTHERMOBAROMETRIC AND HYGROMETRIC CALCULATIONS

Geothermometers or geobarometers are designed to find some chemical balance where there is a significant difference between entropy (ΔS_r) (for a thermometer) or volume (ΔV_r) (for a barometer) of products and reactives (Putirka, 2008). When thermometers or barometers based on equilibrium constants are used, the balance between the phases in question must be considered, for which an equilibrium test can be applied, otherwise the calculated P-T conditions have no meaning (Putirka, 2008).

Olivine, plagioclase, clinopyroxene, and orthopyroxene geothermometers are based on exchange conditions between mineral and melt in equilibrium. Therefore, in order to apply them strictly, only those crystals that do not show evidence of disequilibrium (e.g., sieve textures and reaction rims) can be considered. Thus, calculations based on mineral-liquid equilibria have been limited to compositions obtained in those mineral areas without disequilibrium textures and which are in contact with groundmass (Losantos et al., 2014), assuming that the bulk rock composition roughly represents the magma composition in equilibrium with phases it contains.

In this case, the geochemistry re-calculation presents significant uncertainties, due to the widely described magma mixing, because it is actually difficult to estimate the residual liquid composition before mixing, and the particular composition of this liquid for each crystallization stage in different batches of magma.

Olivine-liquid geothermometer

For estimating the crystallization temperature of olivine in samples of the Nealtican lavas, we chose the olivine-liquid geothermometer based on the exchange of Fe-Mg between the olivine and the liquid where the olivine crystallized. For this, we applied equation 22 from Putirka (2008), which is a modification of the thermometer from Beattie (1993), to correct the systematic overestimation of the temperature.

$$T[°C] = \{15294.6 + 1318.8P(GPa) + 2.4834[P(GPa)]^2\} / \{8.048 + 2.8352\ln(D_{Mg}^{Ol/liq}) + 2.097\ln[1.5\,(C_{MN}^{L})] + 2.575\ln[3(X_{SiO_2}^{liq})] - 1.41NF + 0.222H_2O^{liq} + 0.5P(GPa)\}$$

Where:

$$D_{Mg}^{Ol/liq} = X_{Mg}^{Ol}/X_{Mg}^{liq}$$

$$C_{MN}^{L} = X_{FeO}^{liq} + X_{MnO}^{liq} + X_{MgO}^{liq} + X_{CaO}^{liq} + X_{CoO}^{liq} + X_{NiO}^{liq}$$

$$NF = 7/2 \ln\left(1 - X_{AlO_{1.5}}^{L}\right) + 7\, ln\left(1 - X_{TiO_2}^{L}\right)$$

When using the liquid-olivine thermometer we took the pressure values from Witter et al. (2005) and Roberge et al. (2009), where it is indicated that the pressure estimates in melt inclusions hosted in olivines rarely exceed 400 MPa. Based on this, we took this value as the maximum pressure limit for crystallization of olivine and anhydrous conditions.

Similarly, we assume that the rim composition of the olivine is in balance with a liquid that has the composition of the total rock. In turn, the equilibrium was corroborated considering the exchange coefficient of Fe-Mg, between the olivine and the liquid: $K_D(Fe\text{-}Mg)^{ol\text{-}liq}$=0.30±0.03, which is independent of the temperature and composition. Moreover, we applied an equilibrium test based on the Rhodes diagram (Dungan et al., 1978; Rhodes et al., 1979; Fig A1), where we plotted $Mg\#_{olivine}$ vs. $Mg\#_{liquid}$. The thermometer's estimated precision is ±45ºC.

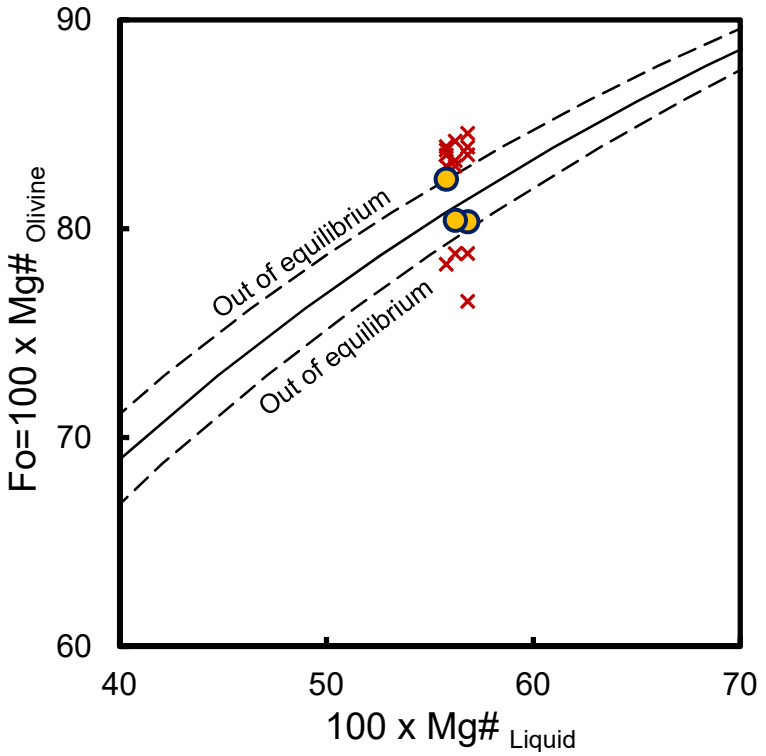

Figure A1. Rhodes diagram of the olivine-liquid equilibrium test. If the olivine crystals are in equilibrium with the co-existing bulk-rock composition, then the assumed liquid-olivine pair should plot along the solid line (yellow circles), within an established error limit, which corresponds to $K_D(Fe\text{-}Mg)^{ol\text{-}liq}$=0.30±0.03, while the olivine crystals falling outside this limit are discarded (red crosses).

Flow 1 (Sample PO09):

The rim of an olivine phenocrystal (Fo_{80}) in equilibrium (K_D=0.32) indicates a temperature of 1125 ºC at 400 MPa.

Flow 1 (Sample PO41):

The rim of an olivine phenocrystal (Fo_{82}) in equilibrium (K_D=0.27) indicates a temperature of 1119 ºC at 400 MPa.

Flow 2 (Sample PO54):

The rims of 2 olivine phenocrystals (Fo_{80}) in equilibrium (K_D=0.31±0.001) indicate a temperature of 1124±0.3 ºC at 400 MPa.

Plagioclase-liquid geothermometer

In order to estimate the temperature of plagioclase crystallization of samples from Nealtican lavas, we chose the plagioclase-liquid geothermometer based on the exchange between the anorthite ($CaAl_2Si_2O_8$) and albite ($NaAlSi_3O_8$) components. We applied the equation 24a from Putirka (2008), considering the presence of water in the liquid (estimated with the hygrometer of Waters and Lange, 2015), thus reducing the systematic errors:

$$\frac{10^4}{\mathrm{T[K]}} = 6.4706 + 0.3128\ln\left[\frac{\mathrm{X_{An}^{pl}}}{\mathrm{X_{CaO}^{liq}}\left(\mathrm{X_{AlO_{1.5}}^{liq}}\right)^2\left(\mathrm{X_{SiO_2}^{liq}}\right)^2}\right] - 8.103\left(\mathrm{X_{SiO_2}^{liq}}\right) + 4.872\left(\mathrm{X_{KO_{0.5}}^{liq}}\right) + 1.5346\left(\mathrm{X_{Ab}^{pl}}\right)^2 + 8.661\left(\mathrm{X_{SiO_2}^{liq}}\right)^2 - 3.341x10^{-2}\left(\mathrm{P(kbar)}\right) + 0.18047\left(\mathrm{H_2O^{liq}}\right)$$

For pressure calculations, the equation 25a from Putirka (2008) could be used:

$$\mathrm{P(kbar)} = -42.2 + 4.94\mathrm{x}10 - 2\mathrm{T(K)} + 1.16\mathrm{x}10 - 2\mathrm{T(K)}\ln\left[\frac{\mathrm{X_{Ab}^{pl}X_{AlO_{1.5}}^{liq}X_{CaO}^{liq}}}{\mathrm{X_{An}^{pl}X_{NaO_{0.5}}^{liq}X_{SiO_2}^{liq}}}\right] - 382.3\left(\mathrm{X_{SiO_2}^{liq}}\right)^2 + 514.2\left(\mathrm{X_{SiO_2}^{liq}}\right)^3 - 19.6\ln\left(\mathrm{X_{Ab}^{pl}}\right) - 139.8\left(\mathrm{X_{CaO}^{liq}}\right) + 287.2\left(\mathrm{X_{NaO_{0.5}}^{liq}}\right) + 163.9\left(\mathrm{X_{KO_{0.5}}^{liq}}\right)$$

Nevertheless, according to Putirka (2008) this pressure estimation is not the most appropriate, because the calibrations did not yield good results, hence we discard it in the present study.

As a possible equilibrium test, we considered the exchange coefficient of Ab-An, between plagioclase and the liquid: $K_D(\mathrm{An\text{-}Ab})^{\mathrm{plg\text{-}liq}}$ = 0.27±0.11.

For water percentage estimates we used the plagioclase hygrometer calibration of Waters and Lange (2015). Calculations were made using a spreadsheet that we downloaded from the American Mineralogist data repository (*http://www.minsocam.org*). Here, we also assumed that plagioclase crystals crystallized in equilibrium with a liquid having a bulk rock composition. In addition, we used temperatures previously obtained with the plagioclase-liquid thermometer and a pressure value of 150 MPa estimated from MELTS simulations with Popocatépetl magmas (Witter et al., 2005). The estimate of the standard error in the hygrometer model is 0.35 wt% H_2O, while the estimated accuracy of the thermobarometer is ±36ºC.

Flow 1 (Sample PO09):

The core of a plagioclase phenocrystal (An_{46}) in equilibrium (K_D=0.24) indicates a temperature of 1069 ºC and 0.9 wt.% H_2O at 150 MPa.

The rim of a plagioclase phenocrystal (An_{43}) in equilibrium (K_D=0.27) indicates a temperature of 1065 ºC and 0.9 wt.% H_2O at 150 MPa.

Flow 1 (Sample PO41):

The core of a plagioclase phenocrystal (An_{49}) in equilibrium (K_D=0.22) indicates a temperature of 1073 ºC and 0.9 wt.% H_2O at 150 MPa.

The rims of two phenocrystals (An_{42-44}) and a micro-phenocrystal (An_{44}) of plagioclase in equilibrium (K_D=0.27±0.01) indicates a temperature of 1064±3.5 ºC and 1.0±0.06 wt.% H_2O at 150 MPa.

Flow 2 (Sample PO54):

The cores of two phenocrystals (An_{42-47}) and a micro-phenocrystal (An_{45}) of plagioclase in equilibrium (K_D=0.26±0.03) indicate a temperature of 1068±5.3 ºC and 0.9±0.06 wt.% H_2O at 150 MPa.

The rim of a plagioclase phenocrystal (An_{46}) in equilibrium (K_D=0.25) indicates a temperature of 1071 ºC and 0.9 wt.% H_2O at 150 MPa.

Flow 3 (Sample PO28):

The cores of a phenocrystal (An_{43}) and two micro-phenocrystals (An_{44-45}) of plagioclase in equilibrium (K_D=0.25± 0.01) indicate a temperature of 1048±1.0 ºC and 1.3 wt.% H_2O at 150 MPa.

The rims of two phenocrystals (An_{41-46}) and a micro-phenocrystal (An_{45}) of plagioclase in equilibrium (K_D=0.25±0.03) indicate a temperature of 1049±2.5 ºC and 1.3 wt.% H_2O at 150 MPa.

Flow 3 (Sample PO32):

The cores of two plagioclase phenocrystals (An_{42-44}) in equilibrium (K_D=0.28± 0.01) indicate a temperature of 1048±1.4 ºC and 1.4 wt.% H_2O at 150 MPa.

The rims of four plagioclase phenocrystals (An_{44-47}) in equilibrium (K_D=0.25±0.02) indicate a temperature of 1055±4.2 ºC and 1.3±0.05 wt.% H_2O at 150 MPa.

Flow 4 (Sample PO18):

The cores of a phenocrystal (An_{45}) and two micro-phenocrystals (An_{42-44}) of plagioclase in equilibrium (K_D=0.24± 0.02) indicate a temperature of 1046±2.5 ºC and 1.3±0.05 wt.% H_2O at 150 MPa.

The rims of three phenocrystals (An_{43-45}) and two micro-phenocrystals (An_{42-44}) of plagioclase in equilibrium (K_D=0.24±0.01) indicate a temperature of 1046±1.1 ºC and 1.3 wt.% H_2O at 150 MPa.

Flow 4 (Sample PO16):

The cores of two phenocrystals (An_{42-45}) and a micro-phenocrystal (An_{46}) of plagioclase in equilibrium (K_D=0.24± 0.02) indicate a temperature of 1044±4.4 ºC and 1.3±0.06 wt.% H_2O at 150 MPa.

The rims of three phenocrystals (An_{38-42}) and a micro-phenocrystal (An_{45}) of plagioclase in equilibrium (K_D=0.26± 0.03) indicate a temperature of 1040±5.1 ºC and 1.4±0.05 wt.% H_2O at 150 MPa.

Clinopyroxene-liquid geothermobarometer

In order to estimate the temperature and pressure of clinopyroxene crystallization of samples from Nealtican lavas, we chose the clinopyroxene-liquid geothermometer. We applied equation 33 from Putirka (2008), considering the presence of water in the liquid (estimated with the hygrometer of Waters and Lange, 2015), thus reducing the systematic errors:

$$\frac{10^4}{T[K]} = 7.53 - 0.14\ln\left[\frac{X_{Jd}^{cpx}X_{CaO}^{liq}X_{Fm}^{liq}}{X_{DiHd}^{cpx}X_{Na}^{liq}X_{Al}^{liq}}\right] + 0.07\left[H_2O^{liq}\right] - 14.9\left[X_{CaO}^{liq}X_{SiO_2}^{liq}\right] - 0.08\ln\left[X_{TiO_2}^{liq}\right]$$
$$- 3.62\left[X_{NaO_{0.5}}^{liq} + X_{KO_{0.5}}^{liq}\right] - 1.1\left[Mg\#^{liq}\right] - 0.18\ln\left(X_{EnFs}^{cpx}\right) - 0.027P(kbar)$$

For pressure estimates we use the equation 32c from Putirka (2008):

$$P(\text{kbar}) = -57.9 + 0.0475T(\text{K}) - 40\left(X_{FeO}^{liq}\right) - 47.7\left(X_{CaTs}^{cpx}\right) + 0.676\left(H_2O^{liq}\right)$$
$$- 153\left(X_{CaO_{0.5}}^{liq} X_{SiO_2}^{liq}\right) + 6.89\left(\frac{X_{Al}^{cpx}}{X_{AlO_{1.5}}^{liq}}\right)$$

Considering the exchange coefficient between Fe-Mg, between clinopyroxene and liquid, a possible equilibrium test is: $K_D(\text{Fe-Mg})_{\text{cpx-liq}}=0.28\pm0.08$ (Fig. A2 A). Additionally, the models of Putirka (1999) are used to predict the equilibrium values for the clinopyroxene components DiHd, EnFs and CaTs (Fig. A2 B). The estimated precision is ±42 °C and ±150 MPa.

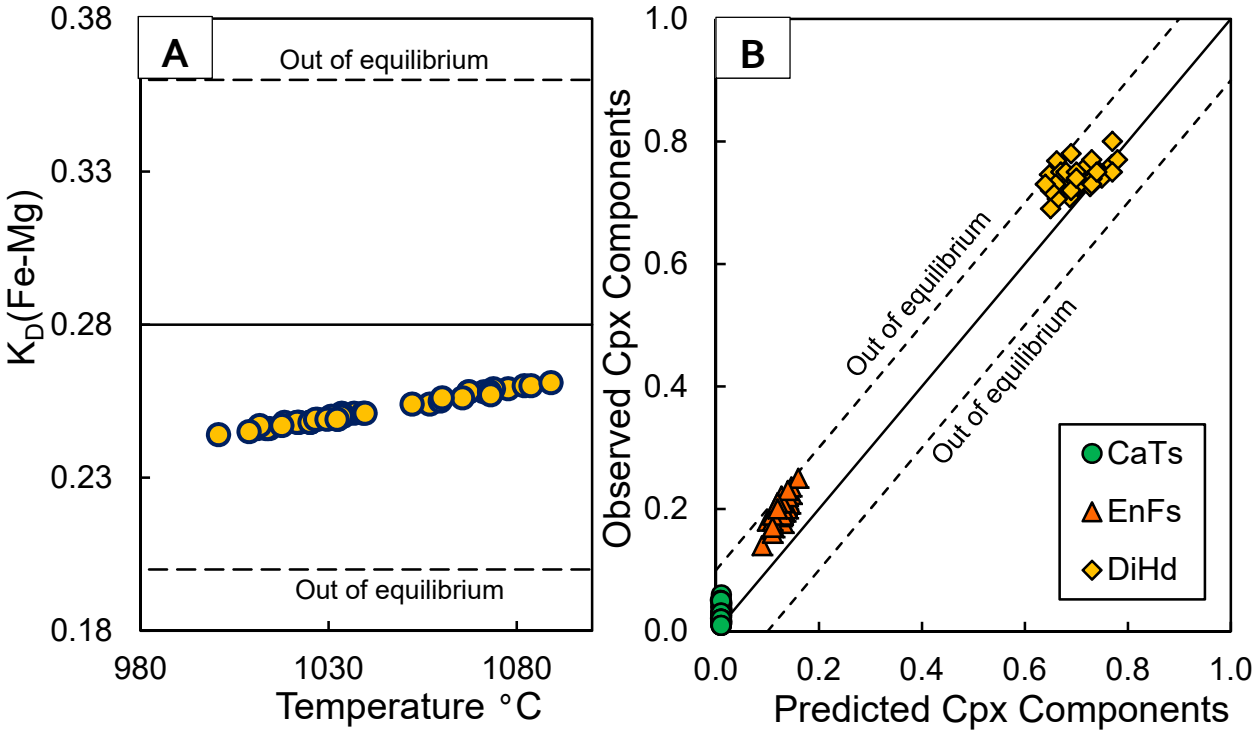

Figure A2. Clinopyroxene-melt equilibrium tests. A. Equilibrium test of $K_D(\text{Fe-Mg})^{\text{cpx-liq}}=0.28\pm0.08$. B. Equilibrium test of DiHd: diopside-hedenbergite, EnFs: enstatite-ferrosilite, and CaTs: Ca-Tschermak components. Equilibrium associated with observed components in pyroxene crystals are paired with predicted components in respective hosting melts (±0.1).

Flow 1 (Sample PO09):

The core of a clinopyroxene phenocrystal in equilibrium ($K_D=0.26$) indicates a temperature of 1074 ºC and 440 MPa with 0.9 wt.% H_2O.

The rims of a phenocrystal and two micro-phenocrystals of clinopyroxene in equilibrium (K_D=0.26±0.001) indicate a temperature of 1076±7.6 ºC and 400±70 MPa with 0.9 wt.% H_2O.

Flow 1 (Sample PO41):

The cores of three clinopyroxene phenocrystals in equilibrium (K_D=0.26±0.001) indicate a temperature of 1071±4.0 ºC and 360±50 MPa with 0.9 wt.% H_2O.

The rims of two phenocrystals and a micro-phenocrystal of clinopyroxene in equilibrium (K_D=0.25±0.001) indicate a temperature of 1056±3.8 ºC and 340±40 MPa with 0.9 wt.% H_2O.

Flow 2 (Sample PO54):

The cores of two clinopyroxene phenocrystals in equilibrium (K_D=0.26±0.004) indicate a temperature of 1075±20.5 ºC and 370±130 MPa with 0.9 wt.% H_2O.

The rims of three clinopyroxene phenocrystals in equilibrium (K_D=0.26±0.001) indicate a temperature of 1074±8.6 ºC and 410±40 MPa with 0.9 wt.% H_2O.

Flow 3 (Sample PO28):

The core of a clinopyroxene phenocrystal in equilibrium (K_D=0.25) indicates a temperature of 1031 ºC and 270 MPa with 1.3 wt.% H_2O.

Flow 3 (Sample PO32):

The core of a clinopyroxene phenocrystal in equilibrium (K_D=0.25) indicates a temperature of 1039 ºC and 260 MPa with 1.4 wt.% H_2O.

The rim of a clinopyroxene phenocrystal in equilibrium (K_D=0.25) indicates a temperature of 1037 ºC and 200 MPa with 1.3 wt.% H_2O.

Flow 4 (Sample PO18):

The rim of a clinopyroxene micro-phenocrystal in equilibrium (K_D=0.25) indicates a temperature of 1034 ºC and 290 MPa with 1.3 wt.% H_2O.

Flow 4 (Sample PO16):

The core of a clinopyroxene phenocrystal in equilibrium (K_D=0.25) indicates a temperature of 1040 ºC and 360 MPa with 1.3 wt.% H_2O.

The rims of two clinopyroxene phenocrystals in equilibrium (K_D=0.25) indicate a temperature of 1034±0.4 ºC and 310±40 MPa with 1.4 wt.% H_2O.

Orthopyroxene-liquid geothermobarometer

For estimating the crystallization temperature and pressure of orthopyroxene in the samples, we chose the orthopyroxene-liquid geothermobarometer. We applied the equation 28a of Putirka (2008), considering the presence of water in the liquid (estimated with the hygrometer of Waters and Lange, 2015), thus reducing the systematic errors:

$$\frac{10^4}{\mathrm{T[°C]}} = 4.07 + 0.329[\mathrm{P(GPa)}] + 0.12\left[\mathrm{H_2O^{liq}}\right] + 0.567ln\left[\frac{\mathrm{X^{opx}_{Fm_2Si_2O_6}}}{\left(\mathrm{X^{liq}_{SiO_2}}\right)^2\left(\mathrm{X^{liq}_{FeO}} + \mathrm{X^{liq}_{MnO}} + \mathrm{X^{liq}_{MgO}}\right)^2}\right] - 3.06\left[\mathrm{X^{liq}_{MgO}}\right] - 6.17\left[\mathrm{X^{liq}_{KO_{0.5}}}\right] + 1.89\left[Mg\#^{liq}\right] + 2.57\left[\mathrm{X^{opx}_{Fe}}\right]$$

For pressure calculations we use the equation 29a from Putirka (2008):

$$\mathrm{P(kbar)} = -13.97 + 0.0129\mathrm{T(°C)} + 0.001416\mathrm{T(°C)ln}\left[\frac{\mathrm{X^{opx}_{NaAlSi_2O_6}}}{\mathrm{X^{liq}_{NaO_{0.5}}X^{liq}_{AlO_{1.5}}}\left(\mathrm{X^{liq}_{SiO_2}}\right)^2}\right] - 19.64\left(\mathrm{X^{liq}_{SiO_2}}\right) + 47.49\left(\mathrm{X^{liq}_{MgO}}\right) + 6.99\left(\mathrm{X^{opx}_{Fe}}\right) + 37.37\left(\mathrm{X^{opx}_{Fm_2Si_2O_6}}\right) + 0.748\left(\mathrm{H_2O^{liq}}\right) + 79.67\left(\mathrm{X^{liq}_{NaO_{0.5}}} + \mathrm{X^{liq}_{KO_{0.5}}}\right)$$

We also assumed that the composition of orthopyroxene rims is in balance with a liquid that has the bulk rock composition. The equilibrium was corroborated by considering the exchange coefficient of Fe-Mg between orthopyroxene and liquid: $K_D(\mathrm{Fe\text{-}Mg})^{opx\text{-}liq}$=0.29±0.06. We were also assisted by an equilibrium test based on the Rhodes diagram (Dungan et al.,1978; Rhodes et al., 1979; Fig. A3), where we plotted the $\mathrm{Mg\#_{Orthopyroxene}}$ vs. $\mathrm{Mg\#_{Liquid}}$. Estimated accuracy is ±39 ºC and ±260 MPa.

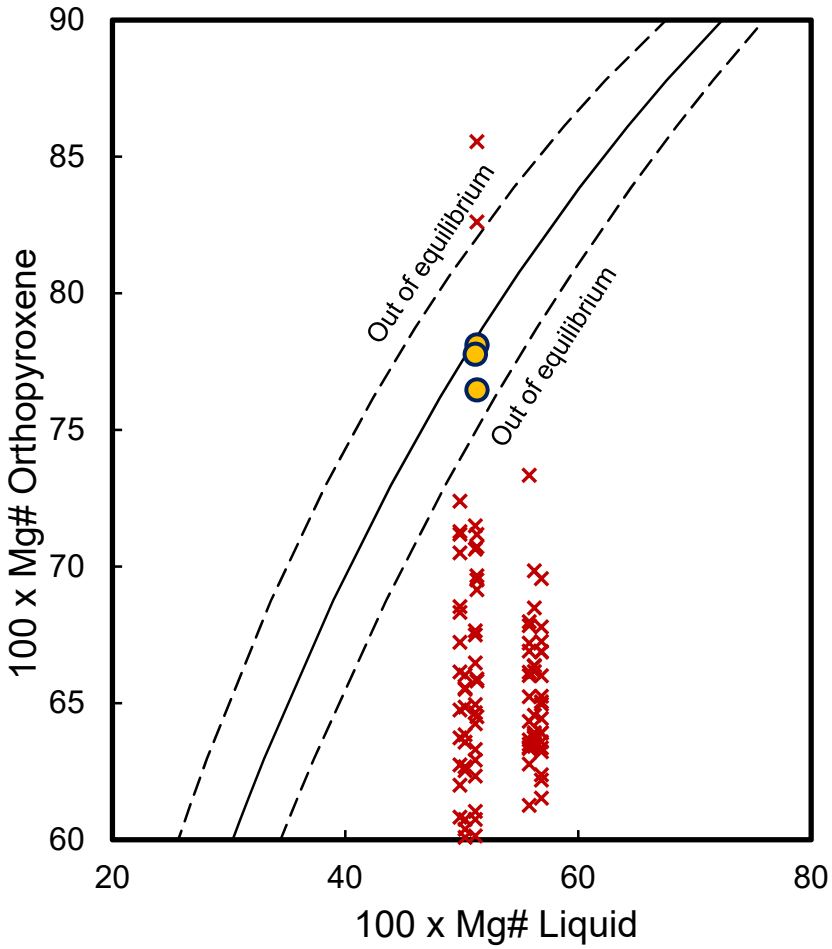

Figure A3. Rhodes diagram of the orthopyroxene-liquid equilibrium test. If the orthopyroxene crystals are in equilibrium with the co-existing bulk rock composition, then the assumed liquid-orthopyroxene pair should plot along the solid line (yellow circles), within an established error limit, which corresponds to $K_D(Fe\text{-}Mg)^{opx\text{-}liq}=0.29\pm0.06$, while the orthopyroxene crystals falling outside this limit are discarded (red crosses).

Flow 3 (Sample PO32):

The core of a phenocrystal and a micro-phenocrystal of orthopyroxene in equilibrium ($K_D=0.31\pm0.01$) indicates a temperature of 1055±1.3 ºC and 250±160 MPa with 1.3 wt.% H_2O.

Flow 4 (Sample PO18):

The core of an orthopyroxene micro-phenocrystal in equilibrium ($K_D= 0.30$) indicates a temperature of 1049 ºC and 310 MPa with 1.3 wt.% H_2O.

Fe-Ti oxides geothermometer

Because chemical diffusion in iron and titanium oxides is very rapid (e.g. Freer and Hauptman, 1978), Fe-Ti oxide geothermometers provide good results by recording temperatures just before an eruption (Takeuchi, 2011). In some cases, a magma mixing temperature can even be estimated just after the magma mixing event (Venezky and Rutherford, 1999). However, Fe-Ti oxides can also be easily rebalanced during the cooling process of lava flows, which makes it difficult to measure the temperature for pre-eruption conditions (Takeuchi, 2011).

In Nealtican lavas we were also able to estimate some temperatures based on the model of the Fe-Ti oxide thermometer by Ghiorso and Evans (2008), which estimates the temperature of magma based on the chemistry of iron-titanium oxide minerals, represented in this case by magnetite and ilmenite. This model can be applied to data sets of natural oxide pairs from siliceous volcanic rocks (Ghiorso and Evans, 2008).

The temperature estimates of this geothermometer can be obtained by using the exchange of $Fe^{+2}Ti \leftrightarrow (Fe^{+3})2$ or $Fe^{+2} \leftrightarrow Mg$ between the two oxides. The estimated accuracy is ±50 °C.

The Fe-Ti oxide geothermometer discussed in Ghiorso and Evans (2008) is available as an online calculator: *http://melts.ofmresearch.org/CORBA_CTserver/OxideGeothrm/OxideGeothrm.php*, which was used in this work.

It should be mentioned that only those pairs in equilibrium between titanomagnetite and ilmenite that passed the Mg/Mn partition equilibrium test from Bacon and Hirschmann (1988) were used.

Flow 4 (Sample PO18):

A pair of magnetite/ilmenite in equilibrium indicate a temperature of 925 ºC.

REFERENCES CITED

Bacon, C. R., and Hirschmann, M. M., 1988, Mg/Mn partitioning as a test for equilibrium between Fe-Ti oxides: American Mineralogist, v. 73, p. 57–61.

Beattie, P., 1993, Olivine-melt and orthopyroxene-melt equilibria: Contributions to Mineralogy and Petrology, v.115, p. 103–111, https://doi.org/10.1007/BF00712982

Dungan, M.A., Long, P.E., and Rhodes, J.M., 1978, Magma mixing at mid-ocean ridges: evidence from legs 45 and 45-DSDP: Geophysical Research Letters, v. 5, p. 423–425, https://doi.org/10.1029/GL005i006p00423

Freer, R., and Hauptman, Z., 1978, An experimental study of magnetite-titanomagnetite interdiffusion: Physics of the Earth and Planetary Interiors, v. 16, p. 223–231, https://doi.org/10.1016/0031-9201(78)90015-8

Ghiorso, M.S., and Evans, B.W., 2008, Thermodynamics of Rhombohedral Oxide Solid Solutions and a Revision of the Fe-Ti Two-oxide Geothermometer and Oxygen-barometer: American Journal of Science, v. 308, p. 957–1039, https://doi.org/10.2475/09.2008.01

Losantos, E., Cebriá, J.M., Morán-Zenteno, D.J., Martiny, B.M., and López-Ruiz, J., 2014, Condiciones de cristalización y diferenciación de las lavas del volcán El Metate (Campo Volcánico de Michoacán-Guanajuato, México): Estudios Geológicos v. 70, p. 1–19, http://dx.doi.org/10.3989/egeol.41589.349

Putirka, K., 1999, Clinopyroxene+liquid equilibrium to 100 kbar and 2450 K: Contributions to Mineralogy and Petrology, v. 135, p. 151–163, https://doi.org/10.1007/s004100050503

Putirka, K.D., 2008, Thermometers and barometers for volcanic systems: Reviews in Mineralogy and Geochemistry, v. 69, p. 61–120, http://dx.doi.org/10.2138/rmg.2008.69.3.

Rhodes, J.M., Dungan, M.A., Blanchard, D.P., and Long, P.E., 1979, Magma mixing at mid-ocean ridges: evidence form basalts drilled near 22°N on the mid-Atlantic ridge: Tectonophysics, v. 55, p. 35–61, https://doi.org/10.1016/0040-1951(79)90334-2

Roberge, J., Delgado-Granados, H., and Wallace, P.J., 2009, Mafic magma recharge supplies high CO_2 and SO_2 gas fluxes from Popocatépetl volcano, Mexico: Geology, v. 37, p. 107–110, https://doi.org/10.1130/G25242A.1

Takeuchi, S., 2011, Preeruptive magma viscosity: An important measure of magma eruptibility: Journal of Geophysical Research, v. 116, p. 1–19, https://doi.org/10.1029/2011JB008243

Venezky, D.Y., and Rutherford, M.J., 1999, Petrology and Fe-Ti oxides reequilibration of the 1991 Mount Unzen mixed magma: Journal of Volcanology and Geothermal Research, v. 89, p. 213–230, https://doi.org/10.1016/S0377-0273(98)00133-4

Waters, L.E., and Lange, R.A., 2015, An updated calibration of the plagioclase-liquid hygrometer-thermometer applicable to basalts through rhyolites: American Mineralogist, v. 100, p. 2172–2184, https://doi.org/10.2138/am-2015-5232

Witter, J.B., Kress, V.C., and Newhall, C.G., 2005, Volcán Popocatépetl, Mexico. Petrology, Magma Mixing, and Immediate Sources of Volatiles for the 1994–Present Eruption: Journal of Petrology, v. 46, p. 2337–2366, https://doi.org/10.1093/petrology/egi058

Supplemental Material 4.

METHODS FOR ESTIMATING RHEOLOGICAL PROPERTIES OF LAVA FLOWS AND THEIR EMPLACEMENT TIMES

Lava viscosity estimated by the petrological approach

The apparent viscosity (η_{app}) of a mixture of polydisperse particles (crystals and bubbles of various shapes and sizes) in a liquid phase (corresponding to silicate melt) can be defined by:

$$\eta_{app} = \eta_{melt} \cdot \eta_r = \eta_{melt}(T, X) \cdot \eta_r(\phi, r, \dot{\gamma}) \qquad (1)$$

where the melt viscosity (η_{melt}) is Newtonian and depends on temperature (T) and composition (X); the relative viscosity (η_r) depends on the volumetric abundance (ϕ) and the particles aspect ratio (r), as well as the flow velocity ($\dot{\gamma}$) (Chevrel et al., 2013).

The interstitial melt viscosity was estimated using the model of Giordano et al. (2008). This model was chosen over other models (e.g. Shaw, 1969; Bottinga and Weill, 1972; Hui and Zhang, 2007) because it considers a wider range of chemical compositions:

$$\log \eta_{melt} = A + \frac{B(X)}{T - C(X)} \qquad (2)$$

where A is a constant representing the lower limit of the silicate melt viscosity at high temperature; and B and C are adjustment parameters depending on the chemical composition (Giordano et al., 2008).

For the estimates we used a spreadsheet available online (*https://www.eoas.ubc.ca/~krussell/VISCOSITY/grdViscosity.html*) in which we input the composition of some glasses (interstitial liquid) that were measured by electron microprobe, as well as the temperatures estimated by geothermobarometry. In turn, we assumed a low dissolved water content (0.1 wt.% H_2O) for the estimation of the interstitial liquid at the time of the eruption, while water content estimated from Waters and Lange (2015) and the bulk groundmass composition obtained by subtracting the phenocrysts chemical composition using the average mass density of the bulk phenocrysts and groundmass was used for magma conditions (see Table A4).

The crystals grow as the magma cools, adding a population of solid particles to the mixture. The relative viscosity was calculated considering a bimodal mixture with fine particles (micro-phenocrysts and microlites) modelled in a bubble-free Newtonian interstitial silicate

melt, taking into account the best fitting parameters of the equations described below, and considering similar aspect ratios to our mineral phases.

The effect of crystals was calculated using the model of Costa et al. (2009), which is useful for high crystal contents. This model is based on a non-Newtonian semi-empirical association for a highly concentrated solid-fluid mixture, taking into account particle shape and strain rate dependence:

$$\eta_r(\phi) = \frac{1+\left(\frac{\phi}{\phi m}\right)^{\delta}}{\left[1-F\left(\frac{\phi}{\phi m},\xi,\gamma\right)\right]^{B\phi m}} \qquad (3)$$

where:

$$F = (1-\xi)erf\left[\frac{\sqrt{\pi}}{2(1-\xi)}\frac{\phi}{\phi_*}\left(1-\frac{\phi^{\gamma}}{\phi_*^{\gamma}}\right)\right] \qquad (4)$$

where ϕ is the crystalline fraction, ϕ_m is the maximum packing, ξ(<<1), δ and γ are empirical parameters that vary according to the strain rate and particle shape, B is the Einstein coefficient (i.e., the intrinsic viscosity;) with a nominal value of 2.5 and ϕ_* is the critical solid fraction where the exponential increase in viscosity begins.

The *erf* error function describes a rheological transition below and above the maximum packing limit. The Costa model is used here with the fitting parameters reported in Cimarelli et al. (2011) based on analogous experiments of polydisperse suspensions including coarse, equidistant, and fine and oblique particles in a bubble-free Newtonian liquid (analogous to interstitial silicate melt). This model allows us to quantify the remaining rheological evolution of the crystalline lava above the critical crystalline fraction where the behaviour of the mixture is controlled by the solid network (Chevrel et al., 2013). Thus, for the samples from the Nealtican lavas, the plagioclase crystals were considered to be angular prolate (aspect ratio of 8.50, maximum packing of 0.32, δ= 12.90, γ= 0.10, ϕ_*=0.24 y ξ= 30×10^{-3}), while pyroxene and olivine crystals were considered angular equant (aspect ratio of 1.82, maximum packing of 0.47, δ= 11.48, γ= 0.69, ϕ_*=0.51 y ξ= 0.05×10^{-3}).

Concerning strain rate, Caricchi et al. (2007) showed experimentally that at relatively low strain rates (10^{-6}-10^{-5} s^{-1}) particle-silicate melt suspensions behave as a Newtonian liquid. Increasing strain rate (ξ), and consequently the applied stress, beyond these values induces a transition to non-Newtonian behavior caused by a decrease of the degree of randomness of the particle distribution (Costa et al., 2009). At high enough strain rates (~10^{-3} s^{-1}), a maximum degree of ordering is reached and the effective viscosity is no longer strain rate-dependent. This high strain rate rheological behavior was observed in several particle-bearing suspensions and was defined as a pseudo-Bingham behaviour (e.g., Barnes, 1999; Costa et al., 2009). In this case we took the calculations estimated at a high deformation rate of 10^{-4} s^{-1}, thus considering that the samples have not a trachytic texture, i.e. the

crystals apparently did not suffer any deformation and were not oriented in a preferential direction, considering the shape and aspect ratio of our crystals.

Effusion rates and emplacement duration estimated from the morphological parameters

Jeffreys equation

Jeffreys (1925) introduced an equation to calculate the average velocity ($\bar{u}$) of a Newtonian liquid flowing in a channel that is much wider than its thickness (5):

$$\bar{u} = \frac{H^2 \rho g \sin\alpha}{3\eta} \quad (5)$$

Here, H is the depth of the lava in the channel, ρ is lava density, g is acceleration due to gravity, α is the angle of the slope down which the lava is flowing and η is the lava viscosity. Here we use this equation where the viscosity is the one obtained from the petrological characterisation.

Note that the Jeffreys equation is for Newtonian fluids, specifically water. Such fluids will flow when an infinitesimal amount of force or shear stress is applied. For a Bingham fluid, however, the shear stress must exceed a critical value before it begins to flow. An alternative method is then to use the equation proposed by Moore (1987).

Grätz-number approach

The lava flow length (L) is related to its velocity (u) through the dimensionless Grätz number (G_z; Knudson and Katz, 1958; Guest et al., 1987; Pinkerton and Wilson, 1994), which considers the ratio of heat advection along the flow length to conductive heat losses (Chevrel et al., 2013):

$$G_z = \frac{uH^2}{kL} \quad (6)$$

where u (m/s) is the mean velocity, k the thermal diffusivity (equivalent to 4.21×10^{-7} m/s^2; Kilburn and Lopes, 1991), H the thickness and L the lava flow length.

Several studies have described the relationship between eruption rate and flow lengths (Walker, 1973; Pinkerton, 1987; Pinkerton and Sparks, 1976; Pinkerton and Wilson, 1994) and have concluded that cooling-limited flows halt when G_z falls in a critical value of 300 (Chevrel et al., 2013). Eruption rate is defined here as values averaged over the flow unit eruption.

Here we assume the equation proposed by Moore (1987) for eruption rate (Q):

$$Q = uWH \quad (7)$$

And we re-organised, using the Eq. 6 and 7 as follows:

$$Q = \frac{G_z k L W}{H} \quad (8)$$

To estimate the emplacement times, we simply divide the flow volume by the eruption rate.

Kerr et al. (2006)

Considering that the flow advance is controlled by the yield strength of a growing crust regime, Kerr et al. (2006) show that the cross-slope flow distance from the channel center-line (i.e., half of the channel width) can be described as a balance between parameters that contribute to flow spreading and the restraints provided by crustal cooling (Deardorff and Cashman, 2012):

$$w = 2\left(\frac{(\rho g)^2 Q^7 \eta^4 cos^9 \alpha}{\tau_c{}^6 k^3 sin^7 \alpha}\right)^{\frac{1}{13}} \quad (9)$$

Here we re-organised Eq. 9 to extract the eruption rate as follows:

$$Q = \left(\frac{\left(\frac{w}{2}\right)^{13} \tau_c{}^6 k^3 sin^7 \alpha}{(\rho g)^2 \eta^4 cos^9 \alpha}\right)^{\frac{1}{7}} \quad (10)$$

Where τ_c is the yield strength of the crust, here we use a τ_c=2×10^6 Pa (best fit of Kerr and Lyman, 2007) and η is the lava viscosity as obtained from the petrological parameters.

Kilburn and Lopes (1991)

Kilburn and Lopes (1991) derived an equation that relates the emplacement time (t_{KL}) to the final dimensions of the flow, independently of the eruption rate, lava intrinsic properties (viscosity, density), and driving forces (gravity) (Chevrel et al., 2016):

$$\frac{W_m}{L_m} H^2 \sin\alpha = nkt_{KL} \quad (11)$$

and therefore:

$$t_{KL=} \frac{W_m H^2 \sin\alpha}{nkL_m} \quad (12)$$

Where W_m and L_m are the maximum width and lava flow length (here we use an average width calculated from various profiles along selected flows), n is a factor equal to 3 for flows with width < depth (inherited from the Jeffreys equation) (Chevrel et al., 2016).

In this model, the motion of the flow's core is treated as steady, uniform, and laminar and behaves as a Newtonian fluid under low deformation rates (Chevrel et al., 2016). Kilburn and Lopes (1991) estimated errors for t are 10% and 70% for $\frac{W_m}{L_m} H^2 \sin\alpha$.

REFERENCES CITED

Barnes, H., 1999, The yield stress-a review or 'panta rei'-everything flows?: Journal of Non-Newtonian Fluid Mechanics, v. 81, p. 133–178, https://doi.org/10.1016/S0377-0257(98)00094-9

Bottinga, Y., and Weill, D.F., 1972, The viscosity of magmatic silicate liquids: A model for calculation: American Journal of Science, v. 272, p. 438–475.

Caricchi, L., Burlini, L., Ulmer, P., Gerya, T., Vassalli, M., and Papale, P., 2007, Non-Newtonian rheology of crystal-bearing magmas and implications for magma ascent dynamics: Earth and Planetary Science Letters, v. 264, p. 402– 419.

Chevrel, M.O., Guilbaud, M.N., and Siebe, C., 2016, The AD 1250 effusive eruption of El Metate shield volcano (Michoacán, Mexico): Magma source, crustal storage, eruptive dynamics, and lava rheology: Bulletin of Volcanology, v. 78, p. 1–32, https://doi.org/10.1007/s00445-016-1020-9

Chevrel, M.O., Platz, T., Hauber, E., Baratoux, D., Lavallée, Y., and Dingwell, D.B., 2013, Lava flow rheology: A comparison of morphological and petrological methods: Earth and Planetary Science Letters, v. 384, p. 109–120, http://dx.doi.org/10.1016/j.epsl.2013.09.022

Cimarelli, C., Costa, A., Mueller, S., and Mader, H.M., 2011, Rheology of magmas with bimodal crystal size and shape distributions: Insights from analog experiments. Geochem: Geochemistry, Geophysics, Geosystems, v. 12, p. 1–14, https://doi.org/10.1029/2011GC003606

Costa, A., Caricchi, L., and Bagdassarov, N., 2009. A model for the rheology of particle-bearing suspensions and partially molten rocks: Geochemistry, Geophysics, Geosystems, v. 10, p. 1–13, https://doi.org/10.1029/2008GC002138

Deardorff, N.D., and Cashman, K.V., 2012, Emplacement conditions of the c. 1,600-year bp Collier Cone lava flow, Oregon: a LiDAR investigation: Bulletin of Volcanology, v. 74, p. 2051–2066, https://doi.org/10.1007/s00445-012-0650-9

Giordano, D., Russell, J.K., and Dingwell, D.B., 2008, Viscosity of magmatic liquids: A model: Earth and Planetary Science Letters, v., 271, p. 123–134.

Guest, J.E., Kilburn, C.R.J., Pinkerton, H., and Duncan, A.M., 1987, The evolution of lava flow-fields: observations of the 1981 and 1983 eruptions of Mount Etna, Sicily: Bulletin of Volcanology, v. 49, p. 527–540, https://doi.org/10.1007/BF01080447

Hui, H., and Zhang, Y., 2007, Toward a general viscosity equation for natural anhydrous and hydrous silicate melts: Geochimica et Cosmochimica Acta, v. 71, p. 403–416.

Jeffreys, H., 1925, The flow of water in an inclined channel of rectangular section: The London, Edinburgh, and Dublin Philosophical Magazine and Journal of Science, v. 49, p. 793–807, https://doi.org/10.1080/14786442508634662

Kerr, R.C., and Lyman, A.W., 2007, Importance of surface crust strength during the flow of the 1988–1990 andesite lava of Lonquimay Volcano, Chile: Journal of Geophysical Research, v. 112, p. 1–8, http://dx.doi.org/10.1029/2006JB004522

Kerr, R.C., Griffiths, R.W., and Cashman, K.V., 2006, Formation of channelized lava flows on an unconfined slope: Journal of Geophysical Research, v. 111, p. 1–13, http://dx.doi.org/10.1029/2005JB004225

Kilburn, C.R.J., and Lopes, R., 1991, General patterns of flow field growth: Aa and blocky lavas: Journal of Geophysical Research, v. 96, p. 19721–19732, https://doi.org/10.1029/91JB01924

Knudson, J.G., and Katz, D.L., 1958, Fluid Dynamics, Heat Transfer: New York, McGraw-Hill, 576 p.

Moore, H.J., 1987, Preliminary estimates of the rheological properties of 1984 Mauna Loa lava: U.S. Geological Survey Professional Paper, 1350, 1569–1588.

Pinkerton, H., 1987, Factor affecting the morphology of lava flows: Endeavour, v. 11, p. 73–79, https://doi.org/10.1016/0160-9327(87)90241-9

Pinkerton, H., and Sparks, R.S.J., 1976, The 1975 sub-terminal lavas, Mount Etna: a case history of the formation of a compound lava field: Journal of Volcanology and Geothermal Research, v. 1, p. 167–182, https://doi.org/10.1016/0377-0273(76)90005-6

Pinkerton, H., and Wilson, L., 1994, Factor controlling the lengths of channel-fed lava flows: Bulletin of Volcanology, v. 6, p. 108–120, https://doi.org/10.1007/BF00304106

Shaw, H.R., 1969, Rheology of basalt in the melting range: Journal of Petrology, v. 10, p. 510–535, https://doi.org/10.1093/petrology/10.3.510

Walker, G.P.L., 1973, Lengths of lava flows: Philosophical Transactions of the Royal Society London, Series A, v. 274, p. 107–118.

Waters, L.E., and Lange, R.A., 2015, An updated calibration of the plagioclase-liquid hygrometer-thermometer applicable to basalts through rhyolites: American Mineralogist, v. 100, p. 2172–2184, https://doi.org/10.2138/am-2015-5232